Assessing Performance of Radar and Visual Sensing Techniques for Ground-To-Air Surveillance in Advanced Air Mobility

Federica Vitiello, Flavia Causa, Roberto Opromolla, Giancarmine Fasano
Department of Industrial Engineering
University of Naples "Federico II"
Naples, Italy
[name.surname]@unina.it

Chester Dolph[1], Todd Ferrante[2]
[1]*Aeronautics Systems Engineering*
[2]*Analytical Mechanics Associates, Inc.*
NASA Langley Research Center
Hampton, VA, USA
chester.v.dolph@nasa.gov
todd.a.ferrante@nasa.gov

Thomas Lombaerts[3], Corey Ippolito[4]
[3]*KBR Wyle Services, LLC*
[4]*Intelligent Systems Division*
NASA Ames Research Center
Mountain View, CA, USA
thomas.lombaerts@nasa.gov
corey.a.ippolito@nasa.gov

***Abstract*— The safe integration of Unmanned Aircraft Vehicles (UAV) within the civil airspace is of great interest to NASA's Advanced Air Mobility project, which envisions high density of operations in and around urban areas that include both UAV and AAM aircraft. To enable safe autonomous operations of both platforms, reliable airspace surveillance strategies must be designed and experimentally validated in relevant scenarios, where multiple small UAV operate flying in low altitude conditions. An example of such a scenario is described in this paper which provides performance assessment of various sensing strategies experimentally tested during flight campaigns with four UAV completing simultaneous missions from vertiports. Such campaigns are performed by the High Density Vertiplex subproject which assesses a prototype of Urban Air Mobility ecosystem. For the purposes of this work, the flights are observed from multiple sensing nodes each with radar and camera sensors. The visual detection and tracking algorithms achieved 96.1% to 99.9% average tracking coverage of the UAV above the horizon, reaching detection ranges larger than 1 kilometer for octocopter. Radar-based tracking shows a lower coverage mainly due to ground clutter removal challenges but provides comparable detection ranges and meter-level range accuracy.**

Keywords—UAV, AAM, UAM, low altitude airspace surveillance, detection and tracking, visual cameras, radars

I. INTRODUCTION

Unmanned Aircraft Vehicles (UAVs) are a fast-developing technology offering an advantageous, promptly deployable and easily scalable alternative to human-based operations. Nevertheless, thanks to the research advancements achieved in this field in the recent years, novel concepts of operations have also flourished. In this context, Advanced Air Mobility (AAM) [1] is among the most promising and revolutionizing concepts, envisioning the exploitation of UAVs for the mobility of people and goods between places which are hardly or less efficiently reached by the traditional aviation means. Such novel transportation paradigm requires highly autonomous operations during Beyond Visual Line Of Sight (BVLOS) flights which are also expected to occur in low altitude conditions. In these latter regards, the term Urban Air Mobility (UAM) [2] can be more properly used to identify a subset of AAM which foresees the air transportation task to be performed in and around urban areas. While UAM package delivery operations have recently become a reality in the U.S., where commercial companies have started their air transportation activities [3], [4], the retrieval of a final, reliable technology allowing the operations of multiple vehicles (*m*) under the control of fewer operators (*N*), also referred to as *m*:*N* [5], is still to be found.

The forecasted dense volumes of operations of UAVs within the AAM/UAM environments as well as their coexistence with the well-established traditional aviation traffic represent considerable challenges to be solved by investigating and adapting all the aspects of the avionics systems that build-up the UAV platform, ranging from navigation to traffic management and surveillance. As an example, many studies have focused on the optimization of path planning algorithms which need to be successfully executed in urban environments, thus accounting for both the complexity of the scenario, where pedestrians and vehicles move [6], as well as the lack or weakening of reliable positioning information provided by the Global Navigation Satellite Systems (GNSS) [7]. At air traffic management level, proofs-of-concept for the integration of UAVs in the civil airspace, respecting the need for flexibility and safety have been proposed [8]. In this context the term Urban Traffic Management (UTM) can be more properly utilized. However, unsolved issues concerning regulations and decisions for all UTM aspects, involving the coordination of operations and airspace structure are still present [9] and are made even harder to be solved if the need for novel infrastructures to also accommodate the take-off and landing of UAVs, i.e., vertiports, is considered [10]. In the field of surveillance, sensing requirements identifying minimum performance standards, airborne and ground-based technologies, algorithmic schemes and air/ground interaction solutions tailored for the different operational environments, safety requirements and flight rules, all present open issues. In this context different strategies can be adopted to tackle the detection and tracking of UAVs. Such strategies can be broadly categorized depending on the location of the chosen sensors' suite (ground-based or airborne) as well as on their nature (active, passive) and on the level of cooperation required (cooperative or non-cooperative) [11].

To this end, NASA Transformational Tools and Technology (TTT) is advancing AAM through the Revolutionary Aviation Mobility (RAM) project with the Autonomous Systems (AS) subproject. Specifically, a distributed sensing system

performing tracking for AAM vertiports and traffic corridors is proposed in [12] and [13]. The proposed autonomous aerial object systems are composed of active and passive sensors, which are particularly useful to monitor the air traffic and detect non-cooperative aircraft that would jeopardize safe, autonomous AAM and UAV operations in the AAM airspace. Indeed, AS and High Density Vertiport (HDV) [14] projects are partnering to develop methodologies for UAV tracking, which can be tailored for AAM aircraft situational awareness, thus easing the timely avoidance of possible collisions with other UAV. Specifically, the HDV architecture relies on cellular and 900 MHz communication links for the broadcasting of status position updates from GNSS and augmented with cellular triangulation. The use of UAVs as proxies for detection, tracking, and classification of AAM aircraft is also of great interest. Prior work includes detecting and tracking multirotor UAV from optical and radar sensors from a single node [15].

Sensors and algorithm research has been carried out in the recent years by the Aerospace Systems research group at the University of Naples "Federico II" (UNINA) to develop Sense and Avoid strategies for small UAVs in low altitude conditions within the "CREATEFORUAS" research project. Specifically, works such as [16] have focused on the performance assessment of fused radar/visual sensing strategies used during ground-to-air experimental flight tests. Such studies have highlighted the need for heterogeneous sensing sources to retrieve reliable tracks of small objects flying close to the ground. Specifically, cameras can provide highly accurate angular information, but their use can be limited by the lack of range measures and the reduced detection performance in poor illumination and bad weather conditions [17]. Radars, on the other hand, can retrieve highly accurate range measures coupled with typically coarser angular information, also strongly dependent on the presence of ground clutter.

The presented work leverages on the previous studies carried out by the authors in past and recent research and is carried out within a collaboration between NASA and UNINA. In the context of this paper, standalone radar and visual strategies are used on data collected during experimental tests whose complexity and added value have been significantly increased with respect to the previous works. A realistic UAM environment, characterized by high density of UAV operations, has been reproduced by exploiting the real flights of four small UAV covering the same path simultaneously and reaching a maximum distance of about 1200 meters with respect to the selected sensors suites. Specifically, two ground-based sensing platforms (referred to as "node 1" and "node 2"), both equipped with a Frequency Modulated Continuous Wave (FMCW) radar and a high-resolution visual camera have been used for traffic monitoring. In this scenario, the current paper provides the following main contributions:

- Development of non-cooperative surveillance algorithms for the low altitude airspace by testing an architecture which does not rely on the broadcasting of vehicles positioning information, also enhancing surveillance in GNSS denied environments.
- Adaptation of the previously developed radar and visual-based sensing strategies to the introduced experimental scenario, defining metrics and benchmarks for performance assessment.
- Comparison of different sensing approaches, thus fostering algorithmic innovations and future developments which also include sensor fusion.

The paper is structured as follows. Section II and III discuss the visual- and radar-based solutions used on the two different nodes. Section IV illustrates the experimental setup and flight scenario. Section V presents the metrics used for the performance evaluation of the retrieved sensing solutions while the experimental results are discussed in Section VI.

II. SENSING STRATEGY ON NODE 1

In this section the visual and radar sensing strategies used on the data retrieved using node 1 will be described. While the two solutions show strong differences in all their constitutive parts, commonalities can be found in both trackers' architecture and track deletion logic. Concerning the former point, each tracker builds up a reliable, i.e., firm (FT), track estimate from tracks of lower confidence, i.e., one-plot (OPT) and tentative (TT) tracks. For each of these, track deletion is performed in absence of associated measurements for a time considered long enough to diminish their reliability level. Therefore, in both solutions tracks are deleted after a time equal to T_{opt}, T_{tt} and T_{ft} for one-plot, tentative and firm tracks, respectively. The latter is typically kept larger than the other two since it is of greatest interest to prevent firm tracks interruptions which could be due to momentaneous losses of measures.

A. Visual-based sensing strategy

The sensing strategy takes its roots from the approach described in [18]. The procedure is briefly recalled hereinafter, while a detailed description can be found in [18]. A detector based on the morphological filtering operator is used to identify the centroids of potential target objects on the image plane, by extracting their pixels coordinates (u,v), which are then fed to the tracker. Such detector is only applied on the image portion falling above the horizon line, which is drawn as to include any fixed object (such as trees and buildings) arising on the horizon. A global thresholding process is then applied on the morphologically filtered image to select regions where objects of interest might be found based on the intensity level of pixels with respect to the background. Then, a local analysis approach is used which computes as statistic of interest the ratio between the intensity in the morphologically filtered image and the standard deviation of the surroundings in the original image.

At tracking level, the state of each detected target is estimated by exploiting two independent, linear, Nearly Constant Velocity (NCV) Kalman filters, which take the detector's measures as input and retrieve the relative position of the UAVs with respect to the camera in terms of the azimuth (az) and elevation (el) angles in the Camera Reference Frame. The tracker is designed as to only perform track propagation, i.e., KF-based track correction and prediction, when a reliable track of the UAV is available. In the lower reliability trackers (one-plot and tentative ones) only measure-to-track association is performed to decide whether the evolution to higher level tracks should be performed. The corresponding condition is based on

the analysis of the Euclidean distance on the image plane between detections in two consecutive frames, as also explained in [19]. For the association to be deemed successful, the computed distance must be smaller than a threshold, τ, whose value is chosen according to the expected maximum motion of the target objects of interest between two subsequent images. Nevertheless, when a firm track is established, the association condition, enabling the usage of a new detection to update the track, is relaxed and shifted to the verification of the presence of the available detection within a region of the image centred around the track prediction and with fixed dimensions of n_{pix}xm_{pix} pixels.

B. Radar-based sensing strategy

The sensing strategy is based on the availability of range (R), azimuth, elevation and range rate ($\dot{R}$) measures which are retrieved by the radar and used as the input of the tracker. In the case of study, the measurements are generated with the radar operating in search-while-track mode, in which agile sensing is exploited to increase the valid measurement rate for existing tracks while scanning the rest of the Field Of View (FOV) for new tracks. Filters on the range rate measure as well as on the estimated Radar Cross Section (RCS) are applied to remove detections arising from ground clutter and isolate those that are more likely to correspond to the small UAVs of interest. Specifically, measures are filtered out if $|\dot{R}| \leq \dot{R}_{th}$ and $RCS_{th,down} \leq RCS \leq RCS_{th,up}$ where $\dot{R}_{th}$ is a threshold applied on the absolute value of the measured range rate and $RCS_{th,down}$ and $RCS_{th,up}$ are the lower and upper limits applied to the estimated RCS, respectively. A similar condition to the RCS one is also used for range measures, thus only retaining those comprised between a minimum and a maximum threshold, indicated as R_{down} and R_{up}, respectively. Clearly, such latter condition can be applied without any significant loss of useful information if some a priori knowledge on the expected flight scenario is available. After measures have been filtered, a centroiding procedure similar to the one described in [20] is applied to cluster all detections that belong to the same object.

The radar tracker is a NCV Extended Kalman filter which transforms the received spherical relative positioning and range rate measures in an estimate of the cartesian relative position of the object with respect to the radar in its Radar Reference Frame. Differently from the camera case, targets' detections frequency is highly variable and depends on the radar revisit time, thus often resulting in a relatively large time interval between two consecutive detections of the same target (easily reaching the order of one second, though being highly dependent on the FOV extensions). This requires the EKF to be used not only in firm tracking mode, but also for TT and OPT steps. The association criterion, which enables such evolution as well as the update of a firm track based on a new measure, exploits the Mahalanobis distance criterion.

III. SENSING STRATEGY ON NODE 2

A. Visual-based sensing strategy

The detection and tracking pipeline on node 2 is an extension of the methodology developed in [21] for tracking a single fixed-wing UAV or General Aviation (GA) aircraft from a multirotor UAV on head-on collision courses above the horizon. The detection strategy employed temporal detection using an image differencing technique and spatial detection using morphological filtering with a 5 by 5 cross-shaped kernel. The tracker uses a linear KF exploiting the Munkres algorithm [22] for measure-to-track association. Specifically, a track can potentially be established if successful association is verified with no more than N_{fail} consecutive dropouts (or fails) over N_{frames}. However, an additional criterion is also added on the total number of associations successfully performed (N_{hits}) within the N_{frames} batch, thus effectively establishing a firm track if the ratio N_{hits}/N_{frames} is greater than or equal to a threshold (vis_{th}). This latter threshold is also used to decide upon the deletion of an already established track which is therefore performed if $(N_{hits}/N_{age}) \leq vis_{th}$, where N_{age} is the number of frames representing the age (or length) of the track. An age requirement parameter, $N_{req\ age}$, sets the minimum amount of updates prior for a track being deleted with the vis_{th} criteria.

Previously, a sensitivity analysis to determine an optimum number of image detections allowed per frame per detector was performed. For the moving camera onboard UAV in low dense airspace, a detection threshold of 5 captured tracking both aircraft across 10 encounters with limited false track generation with only four false tracks over ten sorties and 89.5% tracker coverage for GA and fixed-wing UAV aircraft. Inspection of vertiplex data in this work revealed many birds within the sensor field of view and subsequent analysis using the vision detection and tracking pipeline showed that detection thresholds needed to be adjusted to allow for tracking multiple UAVs, birds, and other aircraft simultaneously in the sensor FOV.

B. Radar-based sensing strategy

As in the case of node 1, the radar mounted on node 2 is also used operating in search-while-track mode, thus enabling the retrieval of different data packets, varying from Constant False Alarm Rate detections to fully processed tracks. Specifically, range, azimuth and elevation estimated by a built-in tracker are comprised within the tracks packet. For the purposes of this work, no specific sensing strategy is applied on the radar of node 2. Indeed, the built-in tracker is used as to also evaluate the capability of the radar to independently track multiple objects flying in low altitude conditions, thus representing a challenging, highly cluttered environment.

IV. EXPERIMENTAL SETUP

A. Flight scenario

The data acquisition carried out for this work was performed during one of the flight days of the HDV NASA subproject, which took place at the NASA Langley City Environment Range Testing for Autonomous Integrated Navigation (CERTAIN) Range flight area [23]. Specifically, on the day of acquisition, four FreeFly Alta 8 platforms UAV flew autonomous missions, thus simulating a complex AAM traffic scenario. The vehicles are shown on the vertiports in Fig. 1. To capture relevant data of the flights, the two nodes were placed in a location that would enable the observation of most of the flights of the UAVs. Thus, a pointing direction of about 88° clockwise from the North and a positive pitch of around 10°

were used. The chosen location is also indicated in Fig. 1, while a snapshot closer to the nodes is given in Fig. 2. Concerning the flight profiles of the UAVs, each vehicle was commanded to complete the same loop, starting and finishing in their respective take-off/landing pads. Such loops, as well as the locations of the ground nodes, are represented in Fig. 3 (top) on a satellite map in latitude/longitude coordinates, retrieved by exploiting the GNSS positioning information logged by the onboard autopilot. On such figure take-off/landing pads location is indicated with the letter V. The altitude (alt) profile of the UAV above the WGS84 ellipsoid with respect to time, is depicted in Fig. 3 (bottom), instead.

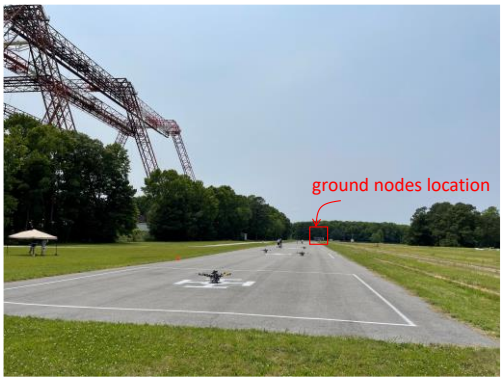

Fig. 1. Snapshot from the flight day. The four Alta 8 can be seen on the runway and the ground nodes location is highlighted within the red box.

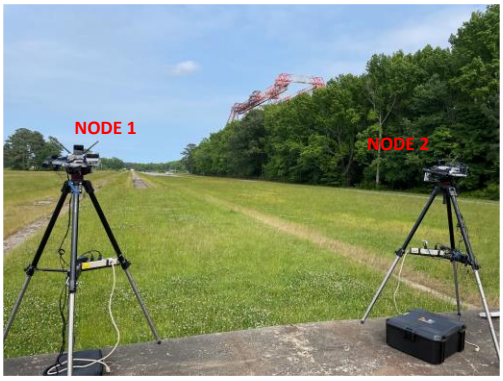

Fig. 2. Snapshot from the flight day. Nodes used during the acquisition.

During the loop completion, taking about 6.5 minutes per vehicle, a total distance of about 1800 meters was traversed by the UAVs reaching a maximum altitude of around 80 meters. For clarity purposes, Fig. 3 only reports one of the vehicles trajectories. To better highlight the multi-vehicle nature of the operations and the temporal succession of each UAVs' mission, the time variation of their range with respect to the location of node 1 is reported in Fig. 4, where the four UAVs are referred to as "NASA UAVs" (NUs) and numbered from 1 to 4, following their take-off sequence. Specifically, the tags numbers corresponding to each NU are reported in the Table I.

TABLE I. TAG NUMBERS OF UAVS

	NU1	***NU2***	***NU3***	***NU4***
Tag Number	N556NU	N557NU	N559NU	N561NU

From this figure the time separation between the vehicles take-off, around 1 minute and 2 minutes for the first three drones and NU4, respectively, can be easily noticed. Indeed, the motion of the NUs with respect to the ground nodes can also be inferred by the behaviour of range shown in Fig. 4. Specifically, the UAVs departed by moving away from the nodes, thus increasing their range from about 400 meters to a maximum of 1230 meters. A decrease in range verified after reaching such maximum distance witnesses the start of the approaching (return) phase, instead.

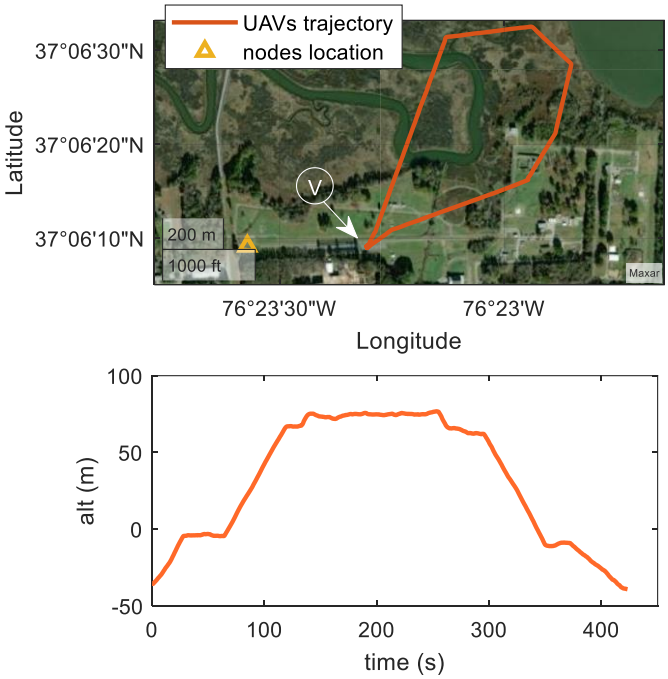

Fig. 3. Satellite map showing the UAVs trajectory (orange line) and the nodes location (yellow triangle) (top). Time variation of UAV altitude with respect to the WGS84 ellipsoid (bottom).

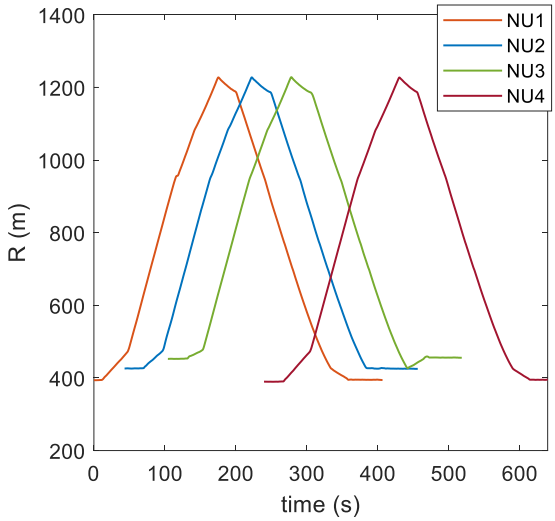

Fig. 4. Time variation of range with respect to the location of node 1 for the four vehicles as estimated from their GNSS position information.

B. *Nodes specifications*

The two nodes share the same hardware architecture at sensor level which comprises the Echodyne's FMCW Echoflight MESA radars, the high-resolution Blackfly S visual cameras from FLIR, and the Ublox F9P GNSS receivers (used to retrieve precise positioning for the nodes as well as a time reference for data synchronization). All these components are highlighted in Fig. 5 for node 1. The radars have a 24 GHz operative frequency with a maximum FOV capacity of 120° in azimuth and 80° in elevation. During the tests, they were configured to operate in the same modality, scanning a fixed FOV whose extension, namely 60° in azimuth and 42° in elevation, was chosen to avoid the inclusion of the tree line surrounding the runway (noticeable in Fig. 1 and Fig. 2). Such FOV is comparable to that of the 12 MegaPixels, global shutter cameras installed on the two nodes, which mount a 12 mm-focal-length optics and an additional lens filter, improving the light transmission, on node 2. Both cameras have a pixel-per-degree of about 81.9. During acquisition, the cameras were set to operate at 10 Hz and 15 Hz on node 1 and 2, respectively.

In terms of processing units, node 1 is equipped with an AMD-64 Intel NUC (11th Gen Intel Core i7 processor and 16GB RAM) while an ARM architecture is mounted on node 2, equipped with a NVIDIA Jetson AGX Xavier board, instead. Both units run the Linux/Ubuntu operative systems.

On a software level, the acquisition on node 1 was performed exploiting the Robot Operating System (ROS). Thus, a unique ROS launch file was written and used to acquire the data from the radar, camera and GNSS receiver altogether. In the case of node 2, two separate C++ software were used to retrieve the camera frames and the radar and GNSS data. All the software versions utilized by the two nodes were designed to also collect CPU times related to the data acquired by each sensor. NASA designed and built both nodes with the input of UNINA for the selection of the Intel NUC.

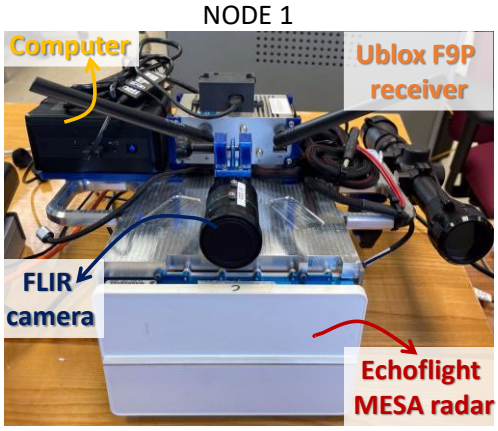

Fig. 5. Node 1 and its constituitve parts.

V. SENSING PERFORMANCE METRICS

Before discussing the results achieved by the sensing strategy tested for each node, this section presents the performance metrics selected for analyses purposes. The percentage of coverage of the UAVs flight path is a common metrics used to assess the performance of both nodes. Specifically, its variation with respect to the detection threshold and tracks age requirement parameter, $N_{req\ age}$, are also provided for node 2. The angular accuracy of the visual sensing solution is also used among the performance metrics for the two nodes, each of which is separately computed for the departure and return phase of the drones' flight. Such accuracy is also reported in terms of range for the radar solution of node 1.

The standalone GNSS information logged by the autopilot onboard each drone (and by the sensing nodes on the ground) is used to generate a Ground Truth (GT). The root mean square (rms) of the difference of each estimated quantity with respect to the corresponding GT one is computed to evaluate the quality of the sensing solution on both nodes. The standalone GNSS GT information is also used to verify the existence of a drone-related firm track in the radar-retrieved tracks. While in the visual case the frames collected by the camera also serve as a reference to evaluate the consistency of the visual tracks, in the radar case no such reference is available. Therefore, a Firm Track (FT) is labelled as a drone-track if the following conditions are met.

$$\begin{aligned} &\left|R_{FT} - R_{GT}\right| \le R_{th,NU} \\ &\left|az_{FT} - az_{GT}\right| \le az_{th,NU} \\ &\left|el_{FT} - el_{GT}\right| \le el_{th,NU} \end{aligned} \quad . \qquad (1)$$

Specifically, $R_{th,NU}$, $az_{th,NU}$, $el_{th,NU}$ are thresholds values set to 10 m, 4° and 6°, respectively. Such values are chosen accordingly to the expected accuracy of the radar track which is then increased by accounting for the GNSS absolute positioning uncertainty. Estimates of the sensors from their reference frame are rotated into GNSS reference frame (North-East-Down) using the QUaternion ESTimation Algorithm (QUEST) [24] to enable a comparison between the sensor estimate and GT.

Track initiation times, which are reported for node 1, are extracted by considering the sensors' FOV limits. Specifically, during departure, the first time when drones appear to be above the horizon are used for the visual case while, for the radar, the take-off time is considered, instead. In the return phase, the first time when the drones appear in each FOV is used as initial time. The track coverage metric on both nodes is also evaluated by following this logic and is computed as the fraction of times when both a drone FT and its corresponding GT are present within the FOVs extensions.

VI. SENSING RESULTS

A. *Visual sensing with node 1*

In the visual case, the tracker uses a 0.1 seconds sampling time. Measure-to-track association is carried out using a 5-pixels threshold for the one-plot and tentative tracks, and setting a 40x50 pixels window during firm tracking, instead. Concerning track deletions, the values of T_{opt}=0.1 s, T_{tt}=0.2 s and T_{ft}=1 s are used. The achieved results in terms of the relative azimuth and elevation angles of the NUs with respect to the camera are shown in Fig. 6 where both GT and FT estimates are depicted. During approximately 10 minutes of tracking, a total number of 99 FTs are generated. The majority of such tracks correspond to birds flying in the FOV of the camera (black lines in Fig. 6).

Indeed, tracks belonging to all four NUs (coloured, thick lines), showing a high accordance with their respective GT, are also reported in the figure. The multi-object nature of the designed tracker is proved by the presence and maintenance of a large number of tracks, corresponding to different objects, simultaneously. However, several points of interruption can be noticed in each track. Such interruptions are to be imputed to the NUs being occluded by the tree line. As an example, Fig. 7 shows two frames captured during different flight phases of NU1. For each frame, a zoom over the region where the drone is located during two different time instants is included to show both the variation in its appearance during the flight and its location with respect to the horizon line (yellow line). The first frame, captured at 168 s, depicts the departure of NU1, which starts at about 5 s and evolves leftwards on the image plane (Northward in the external local reference frame). Specifically, the zoom provided at 168 s, corresponds to few seconds before NU1 disappears from the image plane, due to the occlusion from the trees on the left side of the image. In the return phase of the flight (bottom frame in the figure), the drone moves rightwards (Eastwards), instead, before disappearing below the horizon few seconds after 380 s (zoom on the right). During such phase, track interruptions are also caused by the transit of the drone between trees (visible on the zoom at t=310 s).

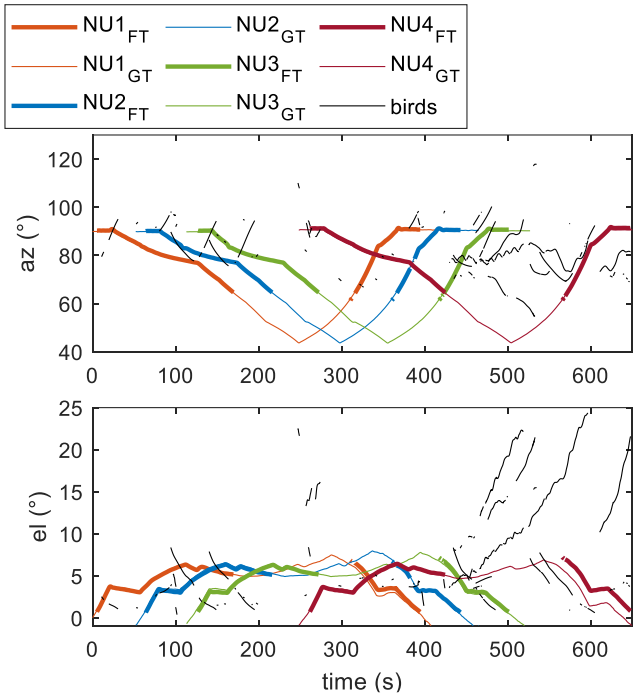

Fig. 6. Results on azimuth (top) and elevation (bottom) from the visual sensing on node 1 reporting both Firm Tracks (FT) and Ground Truth (GT). Tracks of birds are reported in black.

As far as the rms statistics with respect to the GT are concerned, the achieved values are reported in Table II. As it can be noticed, a below-the-degree level of accuracy is reached in all cases but one both in terms of azimuth and elevation. The return phase of NU4 seems to not be reflecting this trend in its elevation component which reaches almost 2° in rms. Still, this occurrence can be traced back to the quality of the GT solution for NU4, which suffers from a decrease in its vertical positioning accuracy if compared to the other drones.

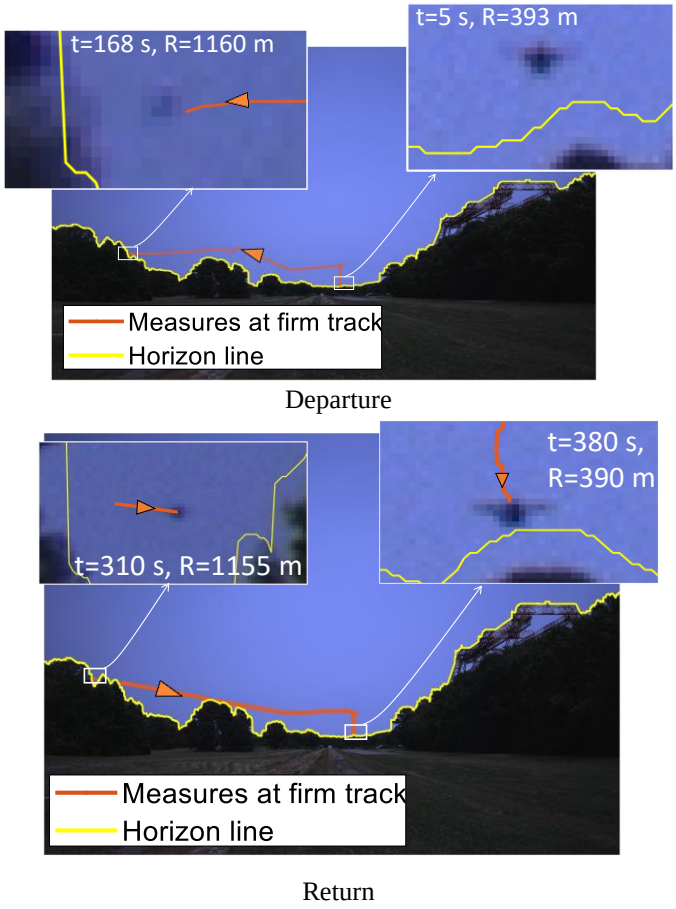

Fig. 7. Collection of camera frames showing different flight phases of NU1. Departure (top), return (bottom). Horizon line, including trees, shown in yellow, detections used to update FT of NU1 shown in orange. Direction of motion is represented with the orange arrows.

TABLE II. VISUAL FIRM TRACKS RMS – NODE 1

	rms az (°), rms el (°)			
	NU1	***NU2***	***NU3***	***NU4***
Departure	0.384°, 0.102°	0.270°, 0.260°	0.344°, 0.236°	0.523°, 0.108°
Return	0.326°, 0.569°	0.238°, 0.137°	0.362°, 0.287°	0.556°, 1.738°

The average time after which tracks are initiated, evaluated with respect to the first appearance of UAVs above the horizon, is of about 0.6 s and 0.4 s during departure and return, respectively. A high track coverage, as high as 99% in most of the cases, is achieved as listed in Table III for all drones. A drop in such coverage value can be noticed for the return phase of NU2 which flies at a slightly lower altitude than the others, thus being more frequently occluded by the trees (as noticeable in the time interval around 380 s in Fig. 8). Concerning the detection range, the exploited detector, applied on the frame retrieved by the camera with about 0.015° Instantaneous FOV, makes it possible to discern the presence of the targeted drones, (with a

dimension of about 1.3 meters) up to a distance of 1150 m, where it occupies a portion of less than 10 pixels.

TABLE III. VISUAL FIRM TRACKS INFORMATION – NODE 1

	Coverage (%)			
	NU1	***NU2***	***NU3***	***NU4***
Departure	99.93%	99.87%	99.86%	100%
Return	99.12%	91.19%	100%	98.88%

B. Radar sensing with node 1

As it has been mentioned in Section II, filtering of radar measures is performed before tracking. The filtering process exploits the threshold values of $RCS_{th,up}$=0 dBsm, $RCS_{th,down}$=-25 dBsm, $\dot{R}_{th}$=1.8 m/s, $R_{th,down}$=350 m and $R_{th,up}$=1200 m. At tracking level, 0.1 s is again chosen as the sampling time for the designed EKF. The achieved results are shown in Fig. 8 where FT estimates and corresponding GT values are reported for azimuth, elevation and range. Unlike in the visual-based case, the radar-based sensing strategy only produces about 15 different FTs. Such difference is a result of the lower ability of the radar to detect the small birds (with smaller RCS values) flying at large distances from the node. Tracks which do not respect the conditions listed in Eq. (1) are labelled as "other" and are shown as black lines in Fig. 8.

Due to the lower number of measures, radar tracks tend to start later than visual ones. Average times at which tracks are generated reach values of 41 s and 13 s during departure and return, respectively. Such difference between the two phases can be explained with a higher number of valid radar measures found when the UAVs are coming back from their loop, as a result of lower ground clutter presence. However, a higher departure flight coverage is achieved, leading to maximum ranges at firm track of about 1200 m in all cases. Still, both departure and return coverages the first being below 89% and the latter below 60%, cannot compare with the visual ones. Coverage values for each UAV are reported in Table IV. Finally, the solution accuracy, evaluated with the rms values reported in Table V, reflects the typical radar-based precise range information, reaching rms values below 5 m, coupled with a coarser angular estimate which, though showing satisfactory levels of accuracy on azimuth (rms no larger than 2.3°), verifies rms values of about 3° in elevation. This trend is verified for both departure and return flight phases. However, in the latter phase, all tracks show divergences phenomena, as especially witnessed by NU4. This is mostly caused by the proximity of the drones to the ground, which complicates the retrieval of valid measures to be used during tracking. As a result, the predicted track more easily associates to detections which plausibly do not correspond to drones. Therefore, to avoid accounting for divergences, the values reported in the return fields of Table V have been cut to the last time when a measure corresponding to the drone is used at firm track. Clearly, while the angular accuracy is not comparable to the visual one, the retrieval of reliable range information, following the flight of the UAVs between 400 m and 1200 m, is an asset of paramount relevance.

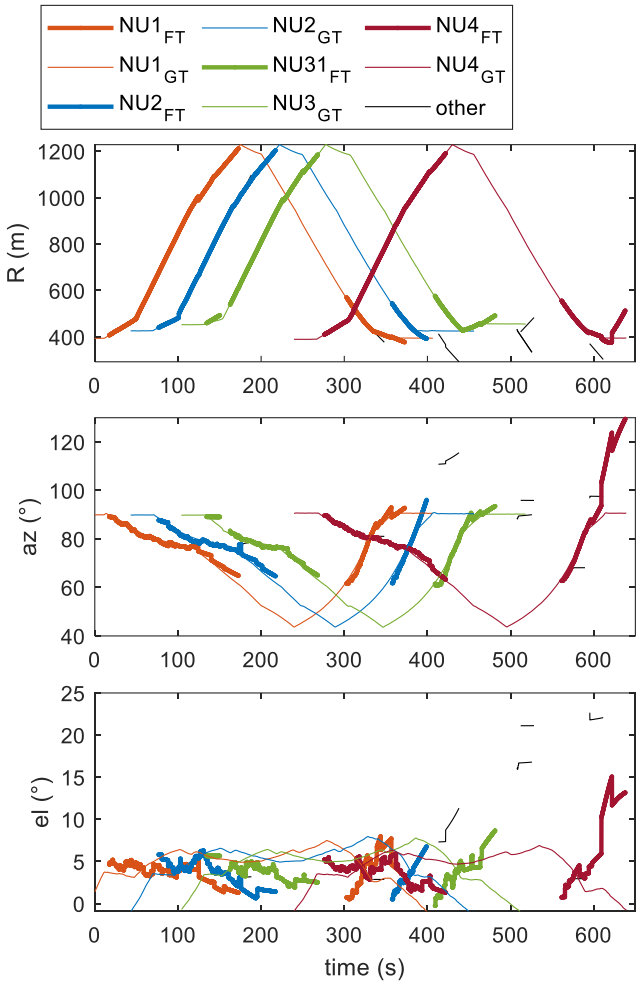

Fig. 8. Results on range (top), azimuth (middle) and elevation (bottom) from the radar sensing on node 1 reporting both Firm Tracks (FT) and Ground Truth (GT). Tracks not associating with the GT are reported in black.

TABLE IV. RADAR FIRM TRACKS INFORMATION – NODE 1

	Coverage (%)			
	NU1	***NU2***	***NU3***	***NU4***
Departure	88.5%	78.8%	69.1%	77.1%
Return	55.98%	36.16%	51.71%	48.81%

TABLE V. RADAR FIRM TRACKS RMS – NODE 1

	rms R (m), rms az (°), rms el (°)			
	NU1	***NU2***	***NU3***	***NU4***
Departure	3.62 m, 1.32°, 2.29°	2.93 m, 1.36°, 2.84°	4.89 m, 1.22°, 2.35°	2.06 m, 0.95°, 2.26°
Return	2.41 m, 1.85°, 3.62°	2.66 m, 2.34 °, 3.32°	3.54 m, 2.25°, 2.89°	3.19m, 2.25 °, 2.75°

VII. SENSING RESULTS WITH NODE 2

A. *Visual sensing with node 2*

Zoomed sample detection results are shown in Fig. 9 for visual detection algorithm, where (a) shows the successful detection of the three UAVs and (b) shows detections of birds. A difference with respect to the appearance of frames captured from node 1 (Fig. 7) can be noticed and is due to the exploitation of the lens filter.

(a)

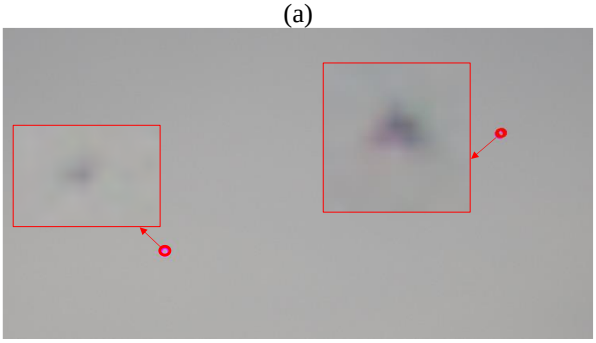

(b)

Fig. 9. Zoomed sample detector output results: (a) NU1, NU2, and NU3 (b) Bird detections.

Concerning tracking results, the exploited settings, mentioned in Section III, are N_{fail}=5 and v_{isth}=0.6.

Tracker coverage results from the parameter search for detection and tracking pipeline are shown in Fig. 10 where the x axis shows the varying detection threshold and $N_{req\ age}$, reported as "NumDetect", and "Age", followed by their numerical values. An ideal tracker optimized for multirotor small UAVs would have 100% ground truth tracker accuracy for detection threshold 5 as there are at most 4 multirotor UAVs in the FOV, however, in addition to multirotor UAVs tracks of birds are also generated and increasing the detection threshold is needed to achieve tracking coverage greater than 90%. A detect, track, and classify methodology may be needed to provide holistic airspace management for shared UAV and manned aircraft airspace. The return phase of the UAV trajectories tends to yield higher ground truth coverage relative to the departure at lower detection thresholds. This is related to the presence of birds and other aircraft in the sensor field of view arising detections.

An assessment of performance across sorties and UAVs is shown in Table VI. Varying age requirement of track resulted in minimal change to ground truth coverage. Increasing the age requirement threshold increases the stability of the reported tracks as they have greater history. A detection threshold of 15 with an age requirement of 30 frames provides 96.1% coverage of the four Alta 8 over departures and returns. These latter settings have been used to evaluate the quality of the visual solution in terms of the rms with respect to the GT. The achieved results are reported in Table VII. As it can be noticed, while azimuth values show a good accordance with the solution retrieved on node 1, elevation rms values show a slight increase, instead. Inspection of visual data has shown that the increase is due to local track divergences caused by the association of detections from birds flying in proximity of the UAV. As in the case of node 1, the highest elevation rms (slightly above 2°) is obtained during the return phase of NU4 and is caused by the degradation of the accuracy in the GT positioning estimate.

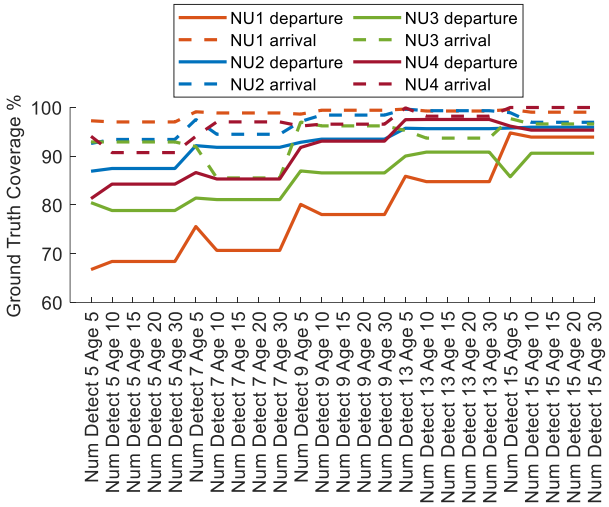

Fig. 10. Tracker coverage for varying Detection Thresholds (NumDetect) and Age Requirement of Track (Age).

TABLE VI. AVERAGE GROUND TRUTH COVERAGE (%) ACROSS ARRIVALS AND DEPARTURES FOR ALL UAV.

Age Requirement \ Detection Thresholds	5	7	9	13	15
5	86.5	89.8	92.6	95.5	96.1
10	86.6	88.1	92.7	94.9	96.1
15	86.6	88.1	92.7	94.9	96.1
20	86.6	88.1	92.7	94.9	96.1
30	86.6	88.1	92.7	94.9	96.1

TABLE VII. VISUAL FIRM TRACKS RMS – NODE 2

	rms az (°), rms el (°)			
	NU1	***NU2***	***NU3***	***NU4***
Departure	0.234°, 0.395°	0.228°, 0.650°	0.186°, 0.349°	0.174°, 0.524°
Return	0.469°, 1.053°	0.433°, 0.797°	0.325°, 0.882°	0.374°, 2.269°

B. *Radar sensing with node 2*

The tracking results achieved by the built-in Echoflight radar tracker are shown in Fig. 11. The estimated range, azimuth and elevation corresponding to each NUs are evaluated by exploiting the conditions in Eq. (1). Clearly, no data pre-processing steps have been performed on the tracks. Thus, to ease the comparison between the two radars' results, the tracks reported in the figure have been selected as those having an estimated range between 350 m ($R_{th,up}$) and 1200 m ($R_{th,down}$).

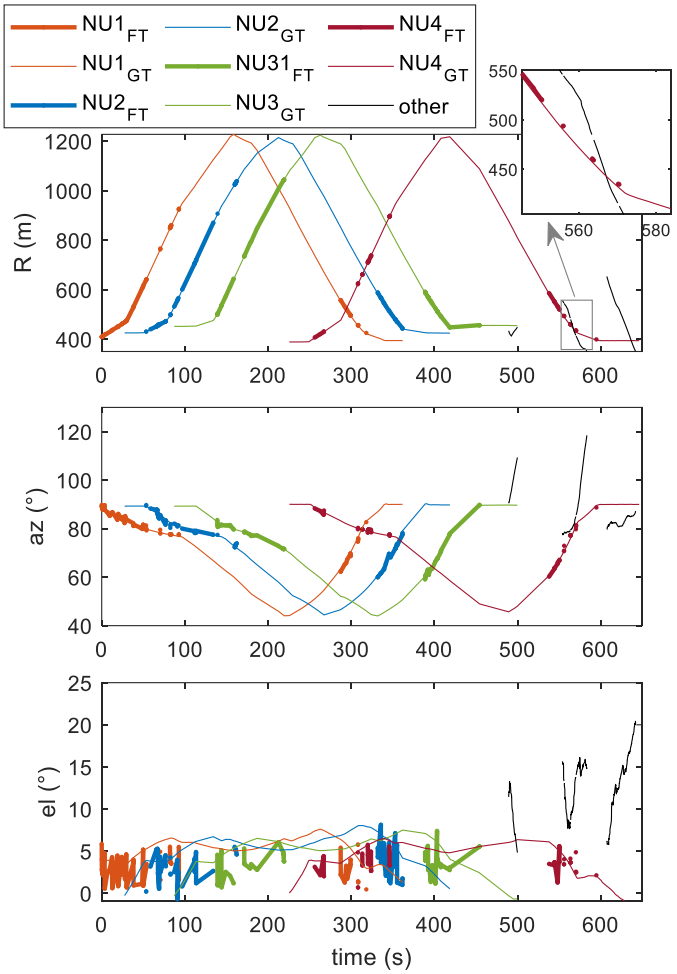

Fig. 11. Results on range (top), azimuth (middle) and elevation (bottom) from the radar sensing on node 2 reporting both Firm Tracks (FT) and Ground Truth (GT). Tracks not associating with the GT are reported in black. A zoom of the range plot (time around 570 s) is provided to highlight the tracks intermittance.

Although the measures retrieved by the radars on both nodes show the expected similarity, a difference exists in the continuity of the estimated tracks. Specifically, a higher intermittency can be observed on the FTs of the latter. This is likely caused by the relation between the complexity of the environment, characterized by a high clutter presence, and the settings used on the tracker, which aggravate its ability to discern objects of interest as well as perform the tracking of multiple targets simultaneously. This is especially visible during the departure of NU4, where highly frequent dropouts occur plausibly due to the return of the previous drones. As a consequence, 93 total tracks are obtained within 10 minutes and an average of 20 independent tracks are generated for each NU. A zoom on the range plot (around a time of 570 s) is also provided in Fig. 11 to highlight the occurrence of localized track dropouts. Departing motion of the NUs is followed up to ranges no higher than 1040 m, where they reach the northern tree line, thus likely being masked by measures in their surroundings.

Focusing on the "other" tracks, a lower frequency of dropouts can be observed. This also validates the idea that objects moving in a less cluttered scenario (higher elevation values) are more easily tracked. Moreover, the time correlation of such tracks with the visual ones demonstrates their belonging to the same birds observed by the camera in the time interval between 500 s and 650 s, thus also proving a higher ability of the tracker to follow fast-moving targets.

VIII. CONCLUSION

In this paper different sensing strategies based on visual and radar information are discussed. The strategies are tested on data retrieved independently by two ground-based sensing nodes during experimental tests which are highly relevant in the framework of AAM surveillance. Four different small UAVs flying a repeated pattern are used as the detection and tracking target to properly test the performance of the designed strategies when multiple small platforms fly together in a low altitude, highly cluttered scenario where other objects, such as birds and other aircraft, are also found. The results have shown that the visual-based solution is typically more capable of offering high track coverage percentage for the two phases of the drones' flights (departure and return). On node 1 an average of 99% coverage is achieved, which is slightly lowered to about 96% in the case of node 2, instead. High detection ranges reaching the kilometer are achieved by the visual strategies on both nodes as a result of the high resolution of the cameras coupled with the physical dimensions of the targets. Indeed, the expected sub-degree accuracy in angular estimates is achieved. In the radar case, the extraction of data of interest to be used during tracking is strongly limited by the complexity of the scenario where fixed obstacles are spread within the radar FOV and drones fly in proximity to the ground. As a consequence, the radar-retrieved solution on node 1 shows a lower track coverage which is due to the lower availability of relevant measures. However, the expected range accuracy (not exceeding 5 meters) is achieved during the motion of UAV from 400 m to 1200 m ranges. Clearly, this information, lacking completely in the camera case, is of paramount relevance, though being coupled with average accuracies on azimuth and elevation of 2° and 3°, respectively. On node 2 the results achieved with the built-in radar tracker show a higher intermittence in the firm tracks of UAVs and a higher tendency to more continuously track fast-moving objects flying higher with respect to the ground. The commonalities between the two nodes' solutions performance clearly show that their hardware settings differences, slightly higher camera acquisition frequency on node 2 which is also equipped with an additional lens filter, do not promote any significant difference on the achieved results.

This work has demonstrated that both radar and visual sensors are able to retrieve information of paramount relevance in the field of the AAM surveillance. Therefore, further

developments will tackle the design of sensor fusion strategies with which an optimal estimate, with accurate range and angular information, can be achieved. Furthermore, the data gathered during the experimental tests have opened up novel scenarios to more properly test distributed sensing strategies where data fusion can be performed by nodes in different locations. Future papers will thus deal with the design and performance assessment of both all-ground and air-ground distributed sensing networks. Finally, real-time solutions will also be targeted in future works by focusing on the needed hardware and software requirements to completely support UAV operations for AAM and UAM.

ACKNOWLEDGMENT

This research was carried out in the frame of project "CREATEFORUAS", funded within Programme PRIN by the Italian Ministry of Education, University and Research. NASA's contribution was completed in support of TTT project milestones. The authors would like to thank the people at NASA Langley that helped making this work possible. Special thanks to Lou Glaab, Jacob Schaffer, Bryan Petty from the HDV team, Matthew Coldsnow, Mark Motter, Patrick Hill, Mark Frye, Jen Fowler, Amanda Neff from the UASOO team, the pilots and ground control station operators Jody Miller, Brayden Chamberlain, Brian Duval, Nicholas Ryder, the visual observers Zackary Mitchell, Aref Malek and Yajvan Ravan. Finally, thanks to Chris Morris and George Szatkowski for their help with radar configuration and analyses.

REFERENCES

[1] "Advanced Air Mobility Project | NASA." https://www.nasa.gov/aeroresearch/programs/iasp/aam/description/ (accessed Jul. 02, 2023).

[2] A. P. Cohen, S. A. Shaheen, and E. M. Farrar, "Urban Air Mobility: History, Ecosystem, Market Potential, and Challenges," IEEE Transactions on Intelligent Transportation Systems, vol. 22, no. 9, pp. 6074–6087, Sep. 2021, doi: 10.1109/TITS.2021.3082767.

[3] "We're Bringing the Convenience of Drone Delivery to 4 Million U.S. Households in Partnership with DroneUp." https://corporate.walmart.com/newsroom/2022/05/24/were-bringing-the-convenience-of-drone-delivery-to-4-million-u-s-households-in-partnership-with-droneup (accessed Jul. 02, 2023).

[4] "UPS Flight Forward, CVS To Launch Residential Drone Delivery Service In Florida Retirement Community To Assist In Coronavirus Response | About UPS." https://about.ups.com/us/en/newsroom/press-releases/innovation-driven/ups-flight-forward-cvs-to-launch-residential-drone-delivery-service-in-florida-retirement-community-to-assist-in-coronavirus-response.html (accessed Jul. 02, 2023).

[5] V. V. Aubuchon, K. E. Hashemi, R. J. Shively, and J. M. Wishart, "Multi-Vehicle (m:N) Operations in the NAS – NASA's Research Plans," in AIAA AVIATION 2022 Forum, American Institute of Aeronautics and Astronautics Inc, AIAA, 2022. doi: 10.2514/6.2022-3758.

[6] T. Castelli, A. Sharghi, D. Harper, A. Tremeau, and M. Shah, "Autonomous navigation for low-altitude UAVs in urban areas," Feb. 2016, [Online]. Available: http://arxiv.org/abs/1602.08141

[7] F. Causa, A. Franzone, G. Fasano "Strategic and Tactical Path Planning for Urban Air Mobility: Overview and Application to Real-World Use Cases". Drones 2023, 7, 11. https://doi.org/10.3390/drones7010011P.

[8] Kopardekar, J. Rios, T. Prevot, M. Johnson, J. Jung, and J. E. R. Iii, "Unmanned Aircraft System Traffic Management (UTM) Concept of Operations," in AIAA Aviation and Aeronautics Forum (Aviation 2016), 2016.

[9] A. Anderegg, L. Vempati, and M. Geffard, "Challenges and Decisions for Near-term Integration of Advanced Air Mobility (AAM) Operations," in AIAA AVIATION 2022 Forum, American Institute of Aeronautics and Astronautics Inc, AIAA, 2022. doi: 10.2514/6.2022-3402.

[10] N. Mendonca, J. R. Murphy, M. D. Patterson, R. Alexander, G. Juárez, and C. Harper, "Advanced Air Mobility Vertiport Considerations: A List and Overview." [Online]. Available: https://arc.nasa.gov/aam-portal/

[11] V. L. Stouffer et al., "Reliable, Secure, and Scalable Communications, Navigation, and Surveillance (CNS) Options for Urban Air Mobility (UAM)," 2020.

[12] Ippolito, Corey A., Kelley E. Hashemi, Evan Kawamura, George E. Gorospe, Wendy Holforty, Keerthana Kannan, Vahram Stepanyan et al. "Distributed Sensing and Advanced Perception Technologies to Enable Advanced Air Mobility." In AIAA SCITECH 2023 Forum, p. 0894. 2023.

[13] Lombaerts, Thomas, Keerthana Kannan, Evan Kawamura, Chester Dolph, Vahram Stepanyan, George E. Gorospe, and Corey A. Ippolito. "Distributed Ground Sensor Fusion Based Object Tracking for Autonomous Advanced Air Mobility Operations." In AIAA SciTech 2023 Forum, p. 0896. 2023.

[14] Glaab, Louis J., Marcus A. Johnson, Robert G. McSwain, Steven C. Geuther, Quang V. Dao, and Jeffrey R. Homola. "The high density vertiplex advanced onboard automation overview." In 2022 IEEE/AIAA 41st Digital Avionics Systems Conference (DASC), pp. 1-10. IEEE, 2022.

[15] Dolph, C., Lombaerts, T., Kawamura, E., Ippolito, C., Stepanyan, V., Iftekharuddin, K., Szatkowski, G., McSwain, R., Morris, C., Malekpour, M., Minwalla, C. (2022). "Ground to air testing of a fused optical-radar aircraft detection and tracking system." In AIAA SCITECH 2022 Forum (p. 0498).

[16] Vitiello, F., Causa, F., Opromolla, R., & Fasano, G. (2022, September). Ground-to-air experimental assessment of low SWaP radar-optical fusion strategies for low altitude Sense and Avoid. In 2022 IEEE/AIAA 41st Digital Avionics Systems Conference (DASC) (pp. 1-10). IEEE.

[17] A. Nussberger, H. Grabner, and L. Van Gool, "Aerial Object Tracking from an Airborne Platform*." in 2014 International Conference on Unmanned Aircraft Systems (ICUAS), 2014.

[18] G. Fasano, D. Accardo, A. E. Tirri, A. Moccia, and E. De Lellis, "Sky Region Obstacle Detection and Tracking for Vision-Based UAS Sense and Avoid," Journal of Intelligent and Robotic Systems: Theory and Applications, vol. 84, no. 1–4, pp. 121–144, Dec. 2016, doi: 10.1007/s10846-015-0285-0.

[19] R. Opromolla and G. Fasano, "Visual-based obstacle detection and tracking, and conflict detection for small UAS sense and avoid," Aerosp Sci Technol, vol. 119, Dec. 2021, doi: 10.1016/j.ast.2021.107167.

[20] Vitiello, F., Causa, F., Opromolla, R., & Fasano, G. (2022, June). Detection and tracking of non-cooperative flying obstacles using low SWaP radar and optical sensors: an experimental analysis. In 2022 International Conference on Unmanned Aircraft Systems (ICUAS) (pp. 157-166). IEEE.

[21] Dolph, C. V., Minwalla, C., Glaab, L. J., Logan, M. J., Danette Allen, B., & Iftekharuddin, K. M. "Detection and Tracking of Aircraft from Small Unmanned Aerial Systems". Journal of Aerospace Information Systems, 18(11), 838-851, 2021.

[22] Munkres, J., "Algorithms for Assignment and Transportation Problems," Journal of the Society for Industrial and Applied Mathematics, Vol. 5, No. 1, 1957, pp. 32–38.

[23] Brown, J. (2016). CERTAIN City Environment Range Testing for Autonomous Integrated Navigation. https://ntrs.nasa.gov/citations/20160009254

[24] M. D. Shuster and S. D. Oh, "Three-axis attitude determination from vector observations", *Journal of Guidance Control and Dynamics*, vol. 4, no. 1, pp. 70-77, 19.